Cgnz1 allele confers kidney resistance to damage preventing progression of immune complex–mediated acute lupus glomerulonephritis

Yan Ge,[1,2,3] Chao Jiang,[1,3] Sun-Sang J. Sung,[1,2] Harini Bagavant,[1,2,4,5] Chao Dai,[1,2] Hongyang Wang,[1,2] Carol C. Kannapell,[1,2] Helen P. Cathro,[6] Felicia Gaskin,[7] and Shu Man Fu[1,2,3]

[1]Division of Rheumatology and Immunology and [2]Center of Immunity, Inflammation and Regenerative Medicine, Department of Medicine; [3]Department of Microbiology, Immunology and Cancer Biology; [4]Division of Nephrology, Department of Medicine; [5]Department of Pharmacology; [6]Department of Pathology; and [7]Department of Psychiatry and Neurobehavioral Sciences, University of Virginia School of Medicine, Charlottesville, VA 22908

***Cgnz1* and *Agnz1* on the distal region of mouse chromosome 1 are associated with chronic glomerulonephritis (cGN) and acute GN (aGN). NZM2328.Lc1R27 (R27) was generated by introgressing a C57L/J region where *Cgnz1* is located to NZM2328. R27 female mice developed aGN mediated by immune complex (IC) deposition and complement activation without progression to cGN with severe proteinuria. End stage renal disease (ESRD) was not seen in R27 mice as old as 15 mo. Thus, aGN and cGN are under separate genetic control, and IC-mediated proliferative GN need not progress to cGN and ESRD. NZM2328 and R27 female mice have comparable immune and inflammatory parameters. In contrast to NZM2328, R27 mice were resistant to sheep anti–mouse GBM serum-induced nephritis, supporting the hypothesis that aGN is mediated by autoimmunity and resistance to the development of cGN is mediated by end organ resistance to damage. Thus, autoimmunity should be considered distinct from end organ damage. The *Cgnz1* region has been mapped to a 1.34 MB region with 45 genes. Nine candidate genes were identified. Clinical relevance of these observations is supported by case studies. Clinical implications and the significance to human lupus and other diseases are presented.**

CORRESPONDENCE
Shu Man Fu:
sf2e@virginia.edu

Abbreviations used: aGN, acute GN; ANA, anti-nuclear Ab; cGN, chronic GN; ESRD, end stage renal disease; GN, glomerulonephritis; IC, immune complex; TEM, transmission electron microscopy.

Systemic lupus erythematosus (SLE) is an autoimmune disorder affecting many organs with circulating autoantibodies of complex specificities (Rahman and Isenberg, 2008; Tsokos, 2011). Kidney is one of the targeted organs resulting in immune complex (IC)–mediated glomerulonephritis (GN). Despite significant progress in therapy, a significant number of patients with lupus GN progress to end stage renal disease (ESRD), requiring dialysis and kidney transplant (Ward, 2009). The treatments of lupus GN involve the use of a combination of steroid and one of the immunosuppressive agents (Hahn et al., 2012). These therapeutic approaches have significant side effects. To provide improved therapy, better understanding of the pathogenesis of lupus GN is needed.

In our previous investigations (Waters et al., 2001, 2004) on the genetics of lupus susceptibility genes in NZM2328 mice, acute GN (aGN) characterized by hypercellularity and focal glomerular necrosis without tubular dilatation or interstitial fibrosis and chronic GN (cGN) characterized by global glomerulosclerosis, tubular dilatation, and marked interstitial fibrosis were used as distinct phenotypes in our genetic analysis. Genes contributing to aGN and cGN

Y. Ge's present address is Genetics Institute, University of Florida, Gainesville, FL 32610.

C. Jiang's present address is Molecular Immunology Section, National Institute of Arthritis and Musculoskeletal and Skin Diseases, National Institutes of Health, Bethesda, MD 20814.

The Rockefeller University Press $30.00
J. Exp. Med. 2013 Vol. 210 No. 11 2387-2401
www.jem.org/cgi/doi/10.1084/jem.20130731

The Journal of Experimental Medicine

are found to be distinct. Of relevance to this investigation is the finding that female mice of the congenic strain NZM2328.Lc1 (Lc1) with a ~26 Mb genetic segment of chromosome 1 transgressed from the non-lupus strain C57L/J to NZM2328 do not have lupus GN. Both *Cgnz1* contributing to cGN and *Agnz1* contributing to aGN are mapped into this 26 Mb segment (Waters et al., 2004). NZM2328.Lc1 provides us the opportunity to determine whether aGN and cGN are under separate genetic control and whether aGN invariably progresses to cGN.

In this investigation, an intrachromosomal recombinant line NZM2328.Lc1R27 (R27) was generated by transgressing an 8 Mb segment of chromosome 1 where *Cgnz1* is located without *Agnz1* from C57L/J to NZM2328. The R27 female mice have IC deposits in the kidney with complement activation and renal pathology characteristic of aGN. However, they do not have severe proteinuria and ESRD. Additional experiments provide evidence that end organ resistance to damage is responsible for this phenotype. These conclusions are congruent with clinical observations.

RESULTS

Generation of NZM.Lc1R8, NZM.Lc1R208-2, and NZM.Lc1R27

In a previous publication (Waters et al., 2001), a single locus, *Cgnz1* on telomeric chromosome 1, was identified to be significantly linked to cGN, severe proteinuria, and early mortality in NZM2328 female mice in the analysis of a backcross cohort of (NZM2328XC57L/J)F1XNZM2328, and three loci were suggestively linked to aGN: *Agnz1* on distal chromosome 1, *Agnz2* on distal chromosome 17, and the *H-2-Tnf* complex. Subsequently, the phenotypes of the congenic line NZM2328.Lc1 (NZM.Lc1 in Fig. 1) support the conclusion that the ~26 Mb genetic segment contributes to the development of both aGN and cGN and the development of antinuclear Abs (ANAs) and anti-dsDNA Abs (Waters et al., 2004). This genetic interval overlaps substantially with *Sle1* (Morel et al., 1994). Breeding of NZM2328.Lc1XNZM2328 generated multiple intrachromosome recombinant lines. Three of them, NZM.Lc1R8 (R8), NZM.Lc1R208-2 (R208-2), and NZM.Lc1R27 (R27), are informative. The phenotypes of R8 were similar to those of NZM.Lc1. In R208-2, the *Agnz1* region was replaced by a homologous region of chromosome 1 from C57L/J. The phenotypes of R208-2 were similar to that of NZM2328 in their development of IC-mediated aGN and cGN, indicating that replacing the susceptible gene *Agnz1* is not sufficient to abolish IC-mediated GN with progression to cGN. R208-2 mice have no detectable circulating ANA and anti-dsDNA Abs. R27 was generated by replacing an 8 Mb (from D1Mit15 to D1Mit166) segment of NZM2328 with that of C57L/J on chromosome 1. In this congenic line, the genetic segment where *Cgnz1* is located was replaced. The phenotypes of R27 female mice were characterized. All studies in this investigation were on female mice.

R27 develops IC-mediated aGN without progression to cGN

As shown in the left panel of Fig. 2 A, a cohort of 15 homozygous R27 female mice was followed up to 12 mo of age for the development of severe proteinuria (>300 mg/dl by dipstick). The incidence of severe proteinuria by 12 mo was 13.3% (2/15). This incidence was significantly lower than that in NZM2328 female mice (72.2%, 26/36, $P = 2 \times 10^{-4}$) but was similar to that in Lc1 female mice (7.3%, 3/41).

Sera from the terminal bleeds of NZM2328, Lc1, R27, and C57L/J female mice were examined for anti-dsDNA Abs and ANA (Fig. 2 A, right). 6.5% (2/31) of the R27 sera and 9.4% (3/32) of the Lc1 sera were positive for IgG anti-dsDNA Abs. The incidence of IgG ANA was 13.8% (4/29) in R27 and 19.2% (5/26) in Lc1 mice. In contrast, 61.1% (22/36) and 53.3% (24/45) of the NZM2328 sera were positive for IgG anti-dsDNA Abs and ANA, respectively. Thus, autoantibody production was reduced in R27 to a similar degree as Lc1 (Waters et al., 2004).

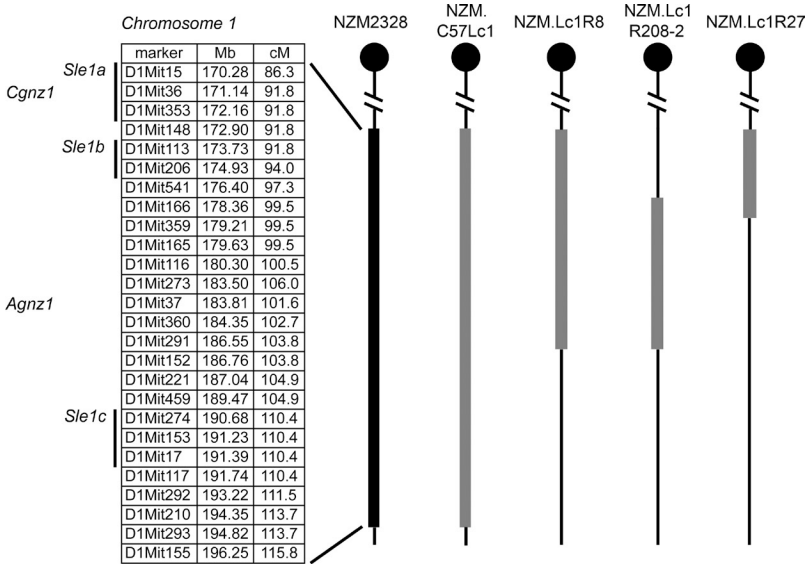

marker	Mb	cM
D1Mit15	170.28	86.3
D1Mit36	171.14	91.8
D1Mit353	172.16	91.8
D1Mit148	172.90	91.8
D1Mit113	173.73	91.8
D1Mit206	174.93	94.0
D1Mit541	176.40	97.3
D1Mit166	178.36	99.5
D1Mit359	179.21	99.5
D1Mit165	179.63	99.5
D1Mit116	180.30	100.5
D1Mit273	183.50	106.0
D1Mit37	183.81	101.6
D1Mit360	184.35	102.7
D1Mit291	186.55	103.8
D1Mit152	186.76	103.8
D1Mit221	187.04	104.9
D1Mit459	189.47	104.9
D1Mit274	190.68	110.4
D1Mit153	191.23	110.4
D1Mit17	191.39	110.4
D1Mit117	191.74	110.4
D1Mit292	193.22	111.5
D1Mit210	194.35	113.7
D1Mit293	194.82	113.7
D1Mit155	196.25	115.8

Figure 1. Genetic composition of chromosome 1 recombinant strains of NZM2328. The gray bars represent the chromosome 1 regions that are replaced in NZM.C57Lc1 (Lc1), NZM.Lc1R8 (R8), NZM.Lc1R208-2 (R208-2), and NZM.Lc1R27 (R27). The listed microsatellite markers based on mouse assembly NCBIM37 were used to determine the boundaries of C57L/J fragments. *Cgnz1* and *Agnz1* loci were mapped to marker D1Mit36 and D1Mit37, respectively. For reference, the *Sle1* subloci (*Sle1a*, *Sle1b*, and *Sle1c*) are illustrated.

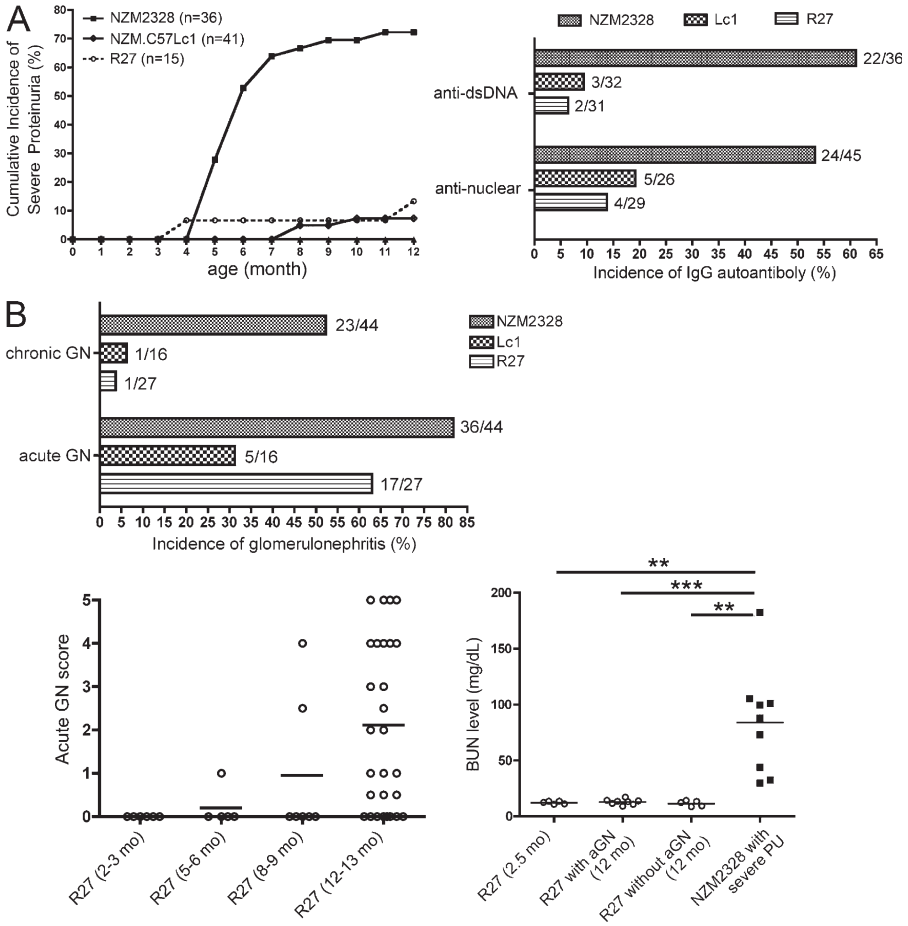

Figure 2. Characterization of cohorts of R27 female mice showing lack of progression of IC-mediated aGN. (A) Severe proteinuria was markedly reduced in R27 (left). Sera from terminal bleeds from NZM2328 or at 12 mo of age from other strains showed that anti-dsDNA and ANA (right) were markedly reduced in R27. (B) cGN was rarely seen in R27 (left). aGN was detected in the majority of the older R27 mice (left and middle). Despite the presence of ICs and complement, renal function of R27 was normal (right). Horizontal bars show means. **, $P < 0.01$; ***, $P < 0.001$.

Histological studies were performed on the kidneys of the cohorts that were sacrificed at 12 mo or when they had severe proteinuria (3–4+ by dipstick) on two consecutive weeks. As shown in the left panel of Fig. 2 B, 63.0% (17/27) of R27 had aGN. This is an incidence that was twice that of Lc1 (31.3%, 5/16) but lower than that of NZM2328 (81.8%, 36/44). In another cohort of R27 female mice, aGN was first observed at the age of 5–6 mo (one out of five mice; Fig. 2 B, middle). The disease severity increased as the mice aged. Compared with R27, NZM2328 mice had a higher incidence (71.4%, 10/14; not depicted) of aGN at 26 wk of age. Despite the development of aGN, R27 had little cGN. Only 1 out of 27 (3.7%) R27 mice developed cGN (Fig. 2 B, left). This incidence was similar to that in Lc1 (6.3%, 1/16) but significantly lower than that in NZM2328 (52.3%, 23/44, $P = 2 \times 10^{-5}$). It is of note that none of the R27 of 13.5–15 mo of age had severe proteinuria or cGN. These histological findings are correlated with renal function in that BUN was not elevated in the R27 mice with aGN (Fig. 2 B, right). Although not shown, another cohort of R27 female mice did not have elevated BUN at the age of 15 mo.

The representative histology of kidneys at 3–4 mo NZM2328 and R27 in comparison with the kidneys of NZM2328 with severe proteinuria and those of R27 with aGN at 12 mo of age are shown in Fig. 3 A. Young R27 and NZM2328 kidneys (Fig. 3 A, 1 and 3) show compact glomeruli with normal tubules. Kidneys of 12-mo-old R27 with aGN (Fig. 3 A, 2) show enlarged glomeruli with dilated capillary loops that contain material stained with PAS. The kidneys of NZM2328 with severe proteinuria (Fig. 3 A, 4) show sclerosed glomeruli with dilated tubules and interstitial infiltration that are consistent with cGN.

Immunofluorescence studies showed that IgM, IgG, IgA, and C3 deposition in R27 female mice occur at 2–3 mo of age (Table 1). These deposits precede the appearance of histological evidence for aGN and coincide with the appearance of circulating antibodies that stain kidneys in a linear fashion (Table 1 and not depicted). The deposits increased in intensity with age. By the age of 12 mo, the intensities of these immune deposits in R27 kidneys were indistinguishable from those in the diseased kidneys of NZM2328. At this time point, a significant portion of the mice have aGN (Table 1). The subclass distribution of the IgG deposits was determined. As shown in Fig. 3 B, there were no qualitative differences among the subclass IgG deposits between the kidneys of NZM2328 (6 mo old) and R27 (12 mo old). In a semiquantitative estimation (Fig. 3 C), IgG2a deposits were similar in kidneys of 12-mo-old R27 and 5–7-mo-old NZM2328 mice, although the mean of staining was higher in NZM2328. Statistically, more IgG1 and IgG2b deposits were found in NZM2328 kidneys

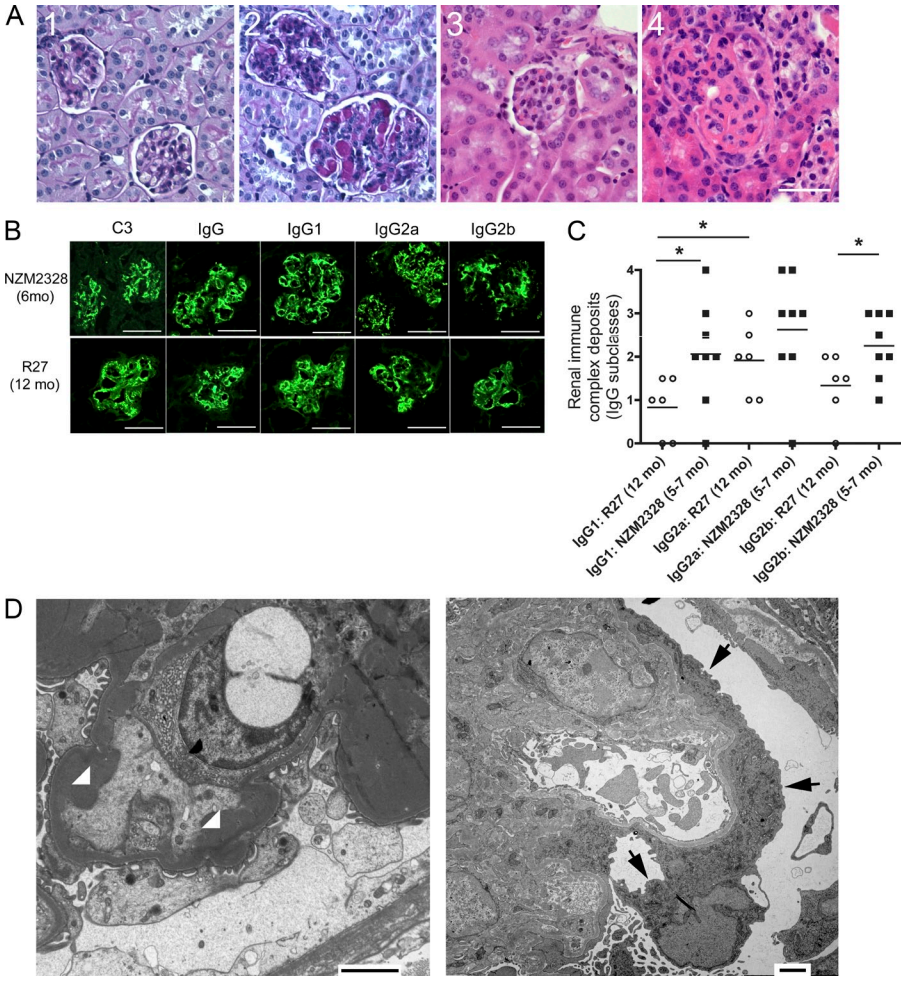

Figure 3. Morphological studies on NZM2328 and R27 kidneys. (A) PAS staining of R27 kidneys and H&E staining of NZM2328 kidneys. R27 females without aGN (1) and with aGN (2) are shown. PAS-positive material in the glomerular capillary lumen is shown in 2. Kidneys of NZM2328 at age of 8 wk and NZM2328 at 36 wk are shown in 3 and 4, respectively. Bar, 50 µm. (B) Immunofluorescent staining for detecting IgG subclasses and C3 in the glomeruli. Bars, 100 µm. (C) Semiquantitative estimates of IgG subclass staining of kidneys of NZM2328 and in R27 at different ages are shown. Horizontal bars show means. *, $P < 0.05$ is denoted by. (D) Transmission electron micrographs of the kidney of a 12-mo-old R27 mouse (left photo; bar, 1 µm) and that of an 8-mo-old NZM2328 mouse (right photo; bar, 5 µm). In the left photo, the arrowheads show subendothelial deposits. Despite the massive deposits, the foot processes are well preserved. In right photo, effacement of the foot processes is shown by the arrows.

in comparison with those of R27. It should be noted that there are significant overlaps between these two groups in all the parameters. Thus, qualitatively there is no subclass IgG dominance in the renal deposits in the kidneys of NZM2328 and R27.

On transmission electron microscopy (TEM), glomeruli of R27 with aGN had numerous large mesangial, subepthelial, and subendothelial electron dense deposits. Fig. 3 D (left photograph) and Fig. 4 D show a 12-mo-old R27 kidney with massive subendothelial deposits. Despite the presence of these deposits, the foot processes of podocytes were intact. In marked contrast, podocyte foot process effacement in NZM2328 diseased kidney was evident (Fig. 3 D, right photo).

IC deposits are cleared by endothelial cells by endocytosis in R27

At the light microscopy level, the morphology of the glomeruli of aged R27 with aGN was very striking in that large dilated capillary loops containing PAS-positive material were seen. By confocal microscopy with collagen V as a surrogate endothelial marker, IgG was identified to be deposited within the lobules within the capillary lumen (Fig. 4, A–C). These dilated loops also contained lipid that was stained with oil red O (unpublished data). It was observed that the appearance of these diluted capillary loops coincides with the appearance of aGN (Table 1).

TEM studies revealed numerous circular structures within the endothelial cells (Fig. 4, E–G). These structures were heterogeneous in their size and electron densities. They were located inside the dilated capillary loops. These unique structures may be formed in the subendothelial space as endocytic vesicles that later fused to generate the large loops. These figures suggest that endothelial cells clear the immune deposits by endocytosis.

Other clinical parameters

Both NZM2328 and R27 female mice had normal blood pressure and normal lipid panel including cholesterol, high density lipoprotein, and low density lipoprotein. They do not have cryoglobulins.

Similar immunological and inflammatory parameters are detected in R27 and NZM2328

Circulating IgM and IgG and its subclasses in R27 and NZM2328 mice were measured at different ages (Table S1).

Table 1. IC deposits and anti-kidney Abs in R27 at different ages

Mouse ID	Age	H&E aGN	Dilated loops	Kidney IgG IC	Kidney IgM IC	Kidney IgA IC	Kidney C3	Staining of B6 kidney IgG	Serum ANA
R27-12	10 wk	0	No	0.5	0	0	1	0.5	-
R27-13	10 wk	0	No	1.5	1.5	2	1	1	-
R27-14	10 wk	0	No	0.5	2	1	1	0.5	-
R27-15	10 wk	0	No	0	2	0	0	0.5	-
R27-16	10 wk	0	No	0.5	1	2	0	1	-
R27-4	3 mo	0	No	1	2	1	1	1	-
R27-19	5 mo	0	No	1	3	1.5	1	2.5	-
R27-20	5 mo	0	No	3	3.5	1.5	1	0.5	-
R27-21	5 mo	0	No	1	3.5	1	1	1	-
R27-17	6 mo	1	No	3	5	2.5	1	0	-
R27-18	6 mo	0	No	1.5	3	2	1	0.5	-
R27-1	12 mo	0	No	3	2.5	4	2	2	-
R27-2	12 mo	0	No	2	2	3	3	2.5	-
R27-7	12 mo	0	No	2	3	0	2.5	1	-
R27-9	12 mo	5	Yes (mild)	3	4	4	2.5	4	-
R27-10	12 mo	4	Yes (mild)	1	4	4	2.5	4	-
R27-11	12 mo	3	Yes (mild)	2.5	2.5	4	3	0	-
R27-3	12 mo	5	Yes	4	4	2	4	1.5	-
R27-6	12 mo	5	Yes	4	5	4	3	0	-
R27-8	12 mo	5	Yes	3	3	4	3	1	-

Scoring is described in Materials and methods.

With increasing ages, serum IgG and IgM levels increase in R27. Comparison of serum IgG and IgG subclasses between 12-mo-old R27 and 5–6-mo-old NZM2328 mice showed significant differences in IgG_1. At 7–9 mo when they had severe proteinuria, the NZM2328 cohort had less IgG1 and more IgG2a than 12-mo-old R27. At 2–3 mo of age, both R27 and NZM2328 had a similar spleen size. In addition, flow cytometric studies showed no differences in lymphocyte populations in the spleens and in the kidney draining lymph nodes in both strains (Table S2). Similar percentages of activated T cells, as measured by the expression of CD69, were detected. The B cell populations of the R27 and NZM2328 mice expressed similar intensities in CD86 staining (Table S2). Similar activation states, as measured by anti-IgM–stimulated Ca^{2+} influx, were detected at 2–3 mo of age, although there were differences in the activation states of B cells of older R27 (8–9 mo) and NZM2328 mice (unpublished data). More importantly, flow cytometric analysis revealed similar numbers of B, T, and dendritic cells and macrophages in the kidneys of 12-mo-old R27 and 7–9-mo-old NZM2328 (unpublished data).

In view of the increasing interest in the role of kidney macrophages and the cytokines made by these macrophages in the pathogenesis of lupus nephritis and renal damage (Schiffer et al., 2008; Bethunaickan et al., 2011), further studies on cytokines made by kidney intrinsic and infiltrating cells, such as endothelial cells, T and B cells, and macrophages, were performed. Q-PCR with RNA isolated from kidney homogenates revealed that the expression of many of the inflammatory and immunological molecules of interest, such as Cxcl13, Cxcr5, Foxp3, Ccr8, IL-10, IL-1β, Pdcd1, Tnf, Vcam1, BAFF (Tnfsf13b), and IL-6, increased with age in R27 and NZM2328 kidneys (Fig. 5). The expression of these molecules varied significantly from one mouse to another. Statistical analysis failed to demonstrate a significant difference between kidneys from R27 mice at 12 mo of age and those from diseased NZM2328 mice (7–9 mo). Similarly, there were no significant differences between kidneys from 8-mo-old R27 and 2-mo-old NZM2328 when there was no histological evidence of cGN.

Macrophage and dendritic cell populations in the kidneys of NZM2328 and R27 were analyzed. Multicolor flow analysis failed to detect differences in macrophages populations at different ages. At ages of 5–6 wk, NZM2328 and R27 mice have similar percentages of dendritic cells and macrophages (Fig. 6 A, top). At later ages, the population of macrophages that expressed F4/80 and intermediate CD11c with I-A were increased in the kidneys of both strains by flow analysis (Fig. 6 B, histograms and bar graph). Staining of kidney sections showed no discernible differences in macrophage populations in the cortex and medulla of diseased NZM2328 and aged R27 (Fig. 6 B, micrographs).

R27 kidneys are resistant to damage by nephrotoxic anti-GBM Abs

Rag1-deficient R27 and NZM2328 were generated to serve as recipients for bone marrow transplantation to determine whether end organ resistance to damage is responsible for the

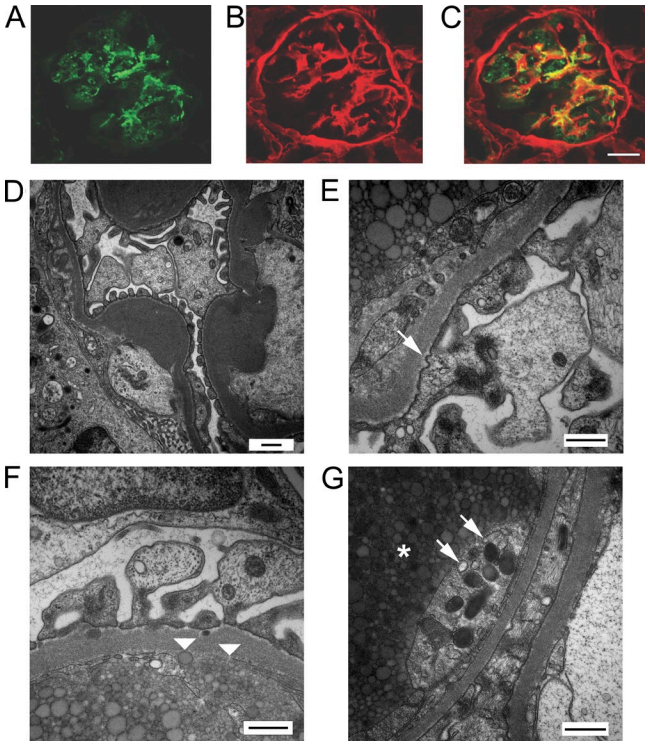

Figure 4. Large capillary loops that represent intracellular vacuoles in the endothelial cells. In A, green fluorescence with FITC-labeled goat F(ab')$_2$ anti–mouse IgG indicates IgG deposits within the glomerulus. In B, collagen V is stained red with PE-labeled goat anti–mouse collagen V. In C, confocal microscopy merging A and B shows intracapillary lumin accumulation of IgG. Bar, 20 µm. D is a TEM (bar, 0.5 µm) of a kidney of a 15-mo-old R27 mouse. Subendothelial electron-dense deposits representing IC deposits are shown. E–G are TEMs (bars, 0.5 µm) of the kidney of a 15-mo-old R27 mouse. In E, the arrow shows the invagination of the podocyte cytoplasmic membrane that may form a small vesicle migrating through the GBM to the subendothelial space. In F, the arrowheads outline the breaking of the endothelial membrane and the formation of the endocytic vesicle within the endothelial cell. In G, the arrows indicate the fusion of a small vesicle with the massive vesicle as denoted by the asterisk within the endothelial cytoplasm.

lack of progression of proliferative GN in R27. All recipients with grafted bone marrow developed thymic lymphoma by the age of 6 mo before the manifestation of severe proteinuria. As an alternative approach, irradiated B27 and NZM2328 were used to create bone marrow chimeras. Because of radiation damage to the kidneys, R27 recipients of syngeneic bone marrow developed significant proteinuria and cGN. Thus, no definitive results were obtained by these two approaches to demonstrate that end organ resistance to damage is responsible, at least in part, for the observed phenotype in R27.

As a third approach, a sheep anti–mouse glomerular basement membrane antiserum (anti-GBM antiserum) was generated. Cohorts of 5–14-wk-old female R27 and NZM2328 mice were given 75 µl anti-GBM antiserum and they were monitored weekly for proteinuria for 4 wk. At the end of the experiment, sera were obtained and kidneys were dissected for histological studies. A second experiment was done in a similar manner. The results of the two experiments were pooled and presented in Fig. 7. As shown in Fig. 7 A, significant proteinuria was detected in NZM2328 7 d after the administration of the anti-GBM antisera. Protein peaked at 21 d. Proteinuria was not detected in any of the R27 recipients (Fig. 7 A), although their glomeruli showed deposits of sheep IgG that were not significantly different in intensity as compared with those in NZM2328 kidneys (Fig. 7 B). Both R27 and NZM2328 mounted comparable immune responses to sheep IgG as demonstrated by the presence of similar titers of anti–sheep IgG Abs (unpublished data). In addition, similar amounts of mouse IgG deposits were detected in the kidneys of both strains (Fig. 7 C). The lack of kidney damage is also demonstrated by the normal histology of the R27 kidneys at the end of the experiments (Fig. 7 D, right photo). In contrast, PAS staining of kidneys from anti-GBM antiserum treated NZM2328 showed enlarged glomeruli with sclerosis and collapsed Bowman's capsules (Fig. 7 D, left photo).

Cgnz1 is located on a 1.34Mb region on chromosome 1

To identify candidate genes for *Cgnz1*, further recombinant lines were generated and characterized. Of the eight recombinant lines of R27, only NZM.Lc1R507-2 (R507-2) is resistant for the progression of aGN to cGN (Fig. 8, top). The susceptibility and resistance to the developments of cGN of these recombinant strains were determined by monitoring a cohort of mice over a period of 12 mo for the development of severe proteinuria (Fig. 8, bottom). These conclusions were confirmed by histology studies (unpublished data). The incidence of ANA of these recombinant strains was <25%. There is no correlation between susceptibility and resistance with ANA incidence. The genotypes and phenotypes of NZM.Lc1R290-2 (R290-2) and NZM.Lc1R507-2 (R507-2) were informative. Although R290-2 mice develop both aGN and cGN with premature death, R507-2 mice have IC-mediated aGN without cGN and progression to ESRD. Further experiments to determine the recombination sites for R507-2 and R290-2 showed that *Cgnz1* is located within a 1.34 Mb of chromosome 1 within the *Sle1b* region. Attempts through more than 2,000 meiotic divisions to generate informative recombinant strains to limit the size of this region further have not been successful.

As shown in the lower panels of Fig. 8, seven of the recombinant lines have higher incidence of severe proteinuria and cGN when compared with NZM2328. This finding indicates that complex epigenetic interactions of certain genes in the R8 regions with *Cgnz1* modulate end organ susceptibility to damage.

This 1.34 Mb region is gene-rich with 45 genes (Table S3). Many of these genes, including the Fc receptors and the genes in the SLAM family, have significant influence on both adoptive and innate immunity. Four of the genes (*Tomm40l*, *Ndufs2*, *Pex19*, and *Casq1*) are mitochondrial genes and three others (*Dedd*, *Itln1*, and *Pea15a*) affect autophagy and cell survival. These seven genes affecting cellular metabolism and cell survival

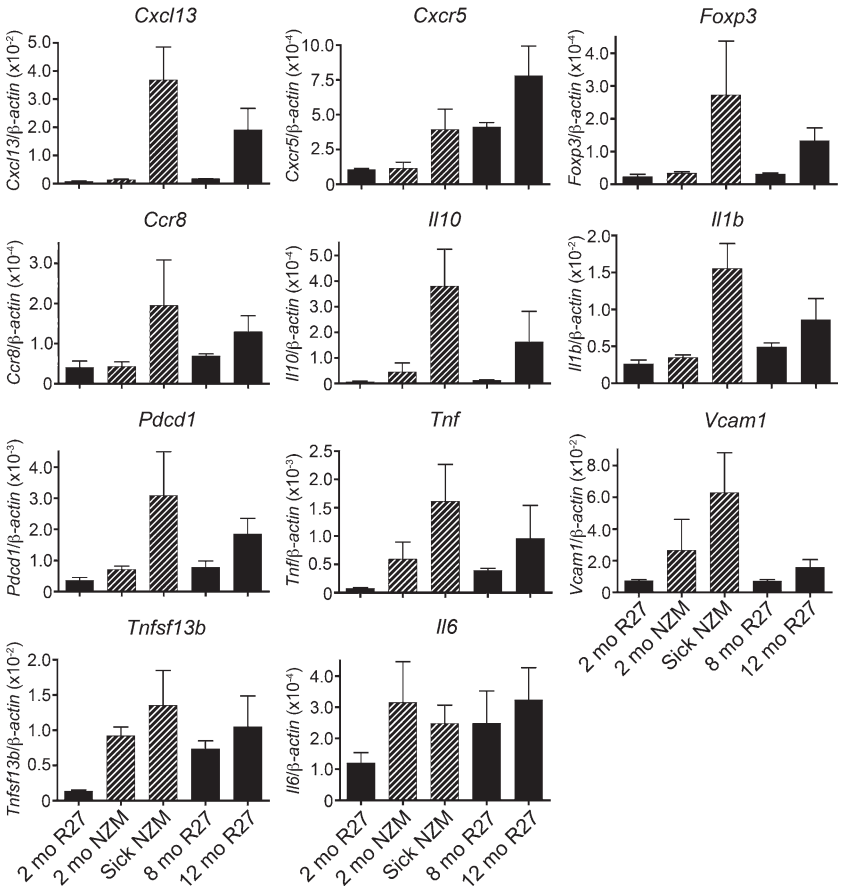

Figure 5. Real-time PCR for mRNA quantitation of mRNA encoding cytokines, chemokines, and their receptors with RNA isolated from renal cortex from three mice of the two strains at various ages. Healthy NZM2328 mice were those at 2 mo of age. Sick NZM2328 (NZM) mice were those that had proteinuria >300 mg/dl detected in two consecutive weeks and their ages were between 6 and 8 mo. R27 mice were used at 2, 8, and 12 mo of age. The primers were those described by Schiffer et al. (2008). Five mice were used for each group. SD was given for each determination.

are likely candidate genes, providing a mechanism for the function of *Cgnz1*. The entire 1.34 Mb region of NZM2328 has been sequenced and the sequence has been compared with that of C57B6, which is available. There are exon nonconservative replacements in *Ndufs2* (46G>C), *Pex19* (1969C>T), and *Itln1* (4735A>C, 16977C>T, 16996T>G, and 17016T>C; Table S4). However, all of these seven genes have replacements in the promoter and intron regions.

Preliminary data were generated regarding the transcriptions of some of these genes. Two of them, *Apoa2* and *1700009P17Rik*, showed clear differences in their mRNA expression between R27 and NZM2328 (unpublished data). As shown in Table S4, both *Apoa2* and *1700009P17Rik* have multiple nucleotide replacement in the promoter regions and in the introns, whereas *Apoa2* has three nonconservative replacements. The amounts of mRNA of these two genes were small. In addition, *Apoa2* has been implicated in atherosclerosis and the function of *1700009P17Rik* remains largely unknown. Thus, it is not clear how they would affect cell survival. Nevertheless, they remain candidates for *Cgnz1*.

Clinical cases showing autoimmunity without end organ damage and end organ resistance to damage preventing the progression of lupus nephritis

Table 2 summarizes four cases of patients who are followed in our clinic and whose clinical courses showed marked heterogeneity among patients with SLE. Although these four cases are anecdotal, they are informative regarding autoimmunity versus end organ resistance to damage. Patient A is a patient with the diagnosis of SLE at the age of 16 yr when she gave birth to a daughter with neonatal skin disease. Over the ensuing 15 yr, she developed hyper-gammaglobulinemia and multiple lupus-related autoantibodies without any symptoms. She represents a group of patients, some of whom have a positive family history for SLE and have evidence for autoimmunity without end organ damage. Patients B and C had proliferative lupus nephritis diagnosed by clinical presentation with hypocomplementemia, proteinuria, and telescopic urinary sediments with red and white cells and casts. Patient B's diagnosis was confirmed by a renal biopsy >1 yr after the onset of proteinuria, and her urine showed red blood cells and casts. The biopsy showed Class III proliferative GN with segmental sclerosis and intact Bowman's capsules without interstitial fibrosis and tubular dilatation. Her IC-mediated aGN did not progress to cGN in >1 yr without treatment. Both patients responded well to therapy. Their clinical course resembles that observed in R27. Patient 4 had rapidly progressive lupus nephritis. Her renal biopsy showed class IV lupus GN with pan-glomerulosclerosis, collapsed Bowman's capsules, interstitial fibrosis, and tubular dilatation. Thus, she presented initially with renal failure and the initial biopsy showed significant chronicity

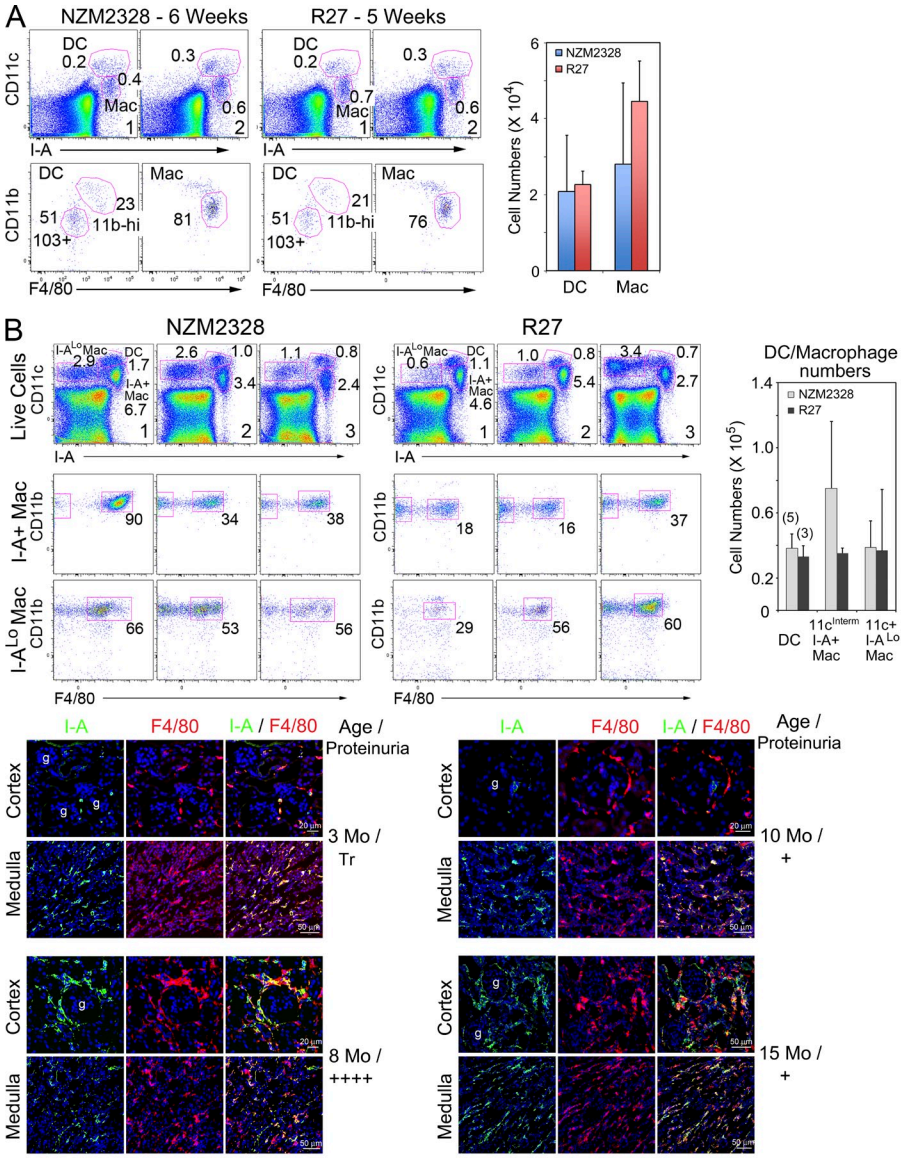

Figure 6. Characterization of renal macrophage and dendritic cell populations in young NZM2328 and R27 mice and in NZM2328 mice with severe proteinuria and 10–15-mo-old R27 mice. (A) Three 6-wk-old NZM2328 and 5-wk-old R27 mice were sacrificed and single cell suspensions were prepared from their kidneys. The renal macrophage and dendritic cell population were studied by flow analysis and the results from two mice are presented on the left and in the middle. The total numbers of macrophages (Mac) and dendritic cells (DCs) per kidney were graphed on the right. SD was provided for these determinations. (B) Percentages of various macrophage and dendritic renal cell populations were determined in three NZM2328 mice with severe proteinuria and three R27 mice (age 10–15 mo) with one to two plus proteinuria by flow cytometry after single cell suspensions were prepared from the kidneys (histograms). The numbers of various macrophages and dendritic cell population per kidney are depicted in the bar graph. Sections of kidney cortex and medulla of NZM2328 and R27 females were stained with anti–I-A and F4/80 mAbs showing comparable macrophage and dendritic cell distributions between 3-mo-old NZM2328 and 10-mo-old R27 (top micrographs, left and right) and between 8-mo-old NZM2328 with severe proteinuria and 15-mo-old R27 with mild proteinuria (bottom micrographs, left and right).

indices. Despite therapy, she developed ESRD requiring dialysis and renal transplantation. Her clinical course resembles that of NZM2328.

DISCUSSION

Genetics of lupus GN

In SLE, kidney is a major target organ for auto-immunological damage. In genetic studies of murine SLE (Theofilopoulos and Dixon 1985), GN is considered to be a single major phenotype with the assumption that proteinuria is caused by IC deposits inevitably linked to ESRD and early mortality. In our initial mapping study, it was observed that aGN and cGN might be under separate genetic control (Waters et al., 2001). It was of note that a locus that contributes significantly to cGN *Cgnz1* was mapped to the same region on chromosome 1 as that for aGN *Agnz1*. This observation was novel and confirmation was required.

In this investigation, a recombinant line R27 has been established in which the region of chromosome 1 that contains the locus *Cgnz1* was replaced by that from C57L/J without replacing the region that encodes *Agnz1*. R27 female mice have aGN with IC and C3 deposition. These mice do not have ESRD and early mortality. These results confirm the genetic mapping data and challenge the current paradigm dealing with IC-mediated lupus nephritis.

Our approach to the genetics of lupus nephritis differs from that of Morel (2012). In the initial mapping for lupus susceptibility genes, *Sle1*, *2*, and *3* were mapped to be associated with GN as the phenotype. These genes were introgressed from the lupus-prone NZM2410 to the non–lupus-prone B6 to generate congenic lines (Mohan et al., 1998). The resulting congenic lines did not show GN. Instead, B6.*Sle1* female mice were shown to have a phenotype of autoimmunity

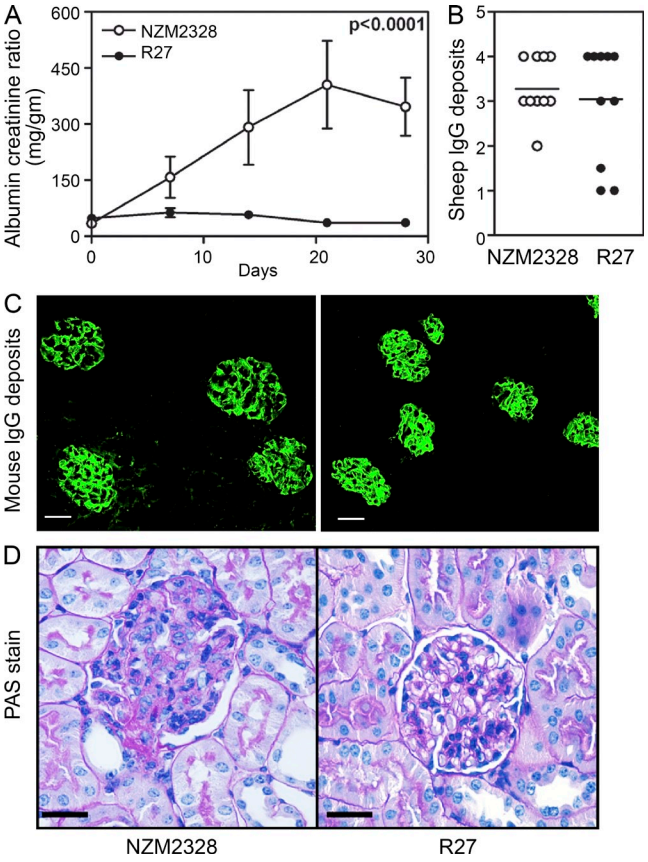

Figure 7. Differential susceptibility of NZM2328 and R27 female mice to the induction of anti-GBM nephritis by sheep anti–mouse GBM antiserum. 10-wk-old NZM2328 and R27 female mice were injected with 75 µl sheep anti-mouse GBM antiserum (nephrotoxic serum) at day zero. Weekly urine samples were collected and their albumin/creatinine ratios were determined. Two cohorts of five mice each for the two groups were followed for 28 d. The data from 10 mice were pooled and are shown. At day 28, mice were sacrificed and their kidneys were studied. (A) Severe proteinuria as measured by urinary albumin/creatinine ratios was detected in NZM2328 as early as 7 d after the injection of the nephrotoxic serum. Error bars represent SD. (B) Similar sheep IgG deposits were detected in the kidneys of each group. Horizontal bars show means. (C) Staining for mouse IgG was detected in the kidneys of both NZM2328 and R27. Bars, 20 µm. (D) PAS staining of the kidneys from anti-GBM antiserum treated NZM2328 and R27. Bars, 50 µm.

with a high proportion of mice making ANA and anti-dsDNA Abs. Furthermore, the phenotypes of bi- and tricongenic strains involving *Sle1*, *2*, and *3* confirm *Sle1* as the most important genetic region in lupus (Morel et al., 2000). In addition, three intrachromosomal congenics, *B6.Sle1a*, *B6.Sle1b*, and *B6.Sle1c*, were generated (Morel et al., 2001). The female mice of all three lines make ANA and anti-dsDNA. Because of the lack of GN in *Sle1* and their subcongenic lines, it was postulated that a genetic locus *Sle1d* exists to account for the GN phenotype. Data from multiple intrachromosomal recombinant lines have mapped *Cgnz1* to a 1.34 Mb region that is colocalized with *Sle1b* (unpublished data). Thus, *Cgnz1* is likely identical to *Sle1d* that is located within *Sle1b*. In addition, *Cgnz1* is likely to be responsible for the observation that NZW (Xie et al., 2003) and NZM2410 (Xie et al., 2013) is susceptible to anti-GBM–induced GN.

There are 45 genes within the region containing *Cgnz1* and no obvious candidate gene is apparent, although one of the SLAM family genes Ly108 that mapped in this region has been claimed to be the gene responsible for hyperactivity of immunocytes (Kumar et al., 2006). Through gene sequence analysis and mRNA expression, nine candidate genes were identified. Four of them are mitochondrial genes and three others are genes affecting autophagy and cell survival. We are in the process of generating transgenic lines with transgenes covering the entire region to further ascertain the genes that may be responsible for the phenotype. We conclude that aGN and cGN are under separate genetic control and that IC deposition with complement activation may not invariably progress to cGN and ESRD. It is important to note that uncoupling IC-mediated aGN from cGN and ESRD in R27 mice suggests that further investigation in the pathogenesis of lupus nephritis is warranted.

End organ resistance to damage is responsible for the nonprogression of lupus GN in R27 mice

The dissociation of IC deposition and complement activation has been reported (Clynes et al., 1998). In B/WF1 female mice that lack the γ chain of the Fc receptor, IgG and C3 deposits were demonstrated in the kidney without cGN and early death. The circulating IgM and IgG, as well as IgG subclasses with anti-dsDNA specificities, were not different between $\gamma^{-/-}$ and $\gamma^{+/-}$ mice. In the absence of Fc γRIII, end organ damage was not detected. Thus, effector function deficiency is responsible for the observed uncoupling.

Genetic manipulation to shift the autoimmune responses to Th2 has been reported (Shimizu et al., 2005; Jacob et al., 2006) to uncouple immune deposits from renal damage. In the MRL/*lpr.IL27R*$^{-/-}$ mice, Shimizu et al. (2005) showed a significant decrease in anti-dsDNA antibodies, and serum IgG_1 and IgE were increased with a decrease in circulating IgG_{2a}. There were fewer renal deposits of IgG_{2a}. The IL27R-deficient mice had membranous GN with prolonged survival. In the study by Jacob et al. (2006), female NZM2328.*Baff*$^{-/-}$ mice had strong IgG_1 deposits in the kidney without complement activation and without severe proteinuria. More than 90% of the females survived >12 mo despite the presence of class IV disease of proliferative GN.

In R27 mice with intact FcR, the uncoupling of IC-mediated nephritis from severe proteinuria, cGN, and early mortality is not due to the lack of effector function. Although there was significantly more serum IgG_1 and less IgG_{2a} in aged R27, this Th2 shift is of uncertain significance in that R27 kidneys had deposits of all IgG subclasses and C3 activation. Thus, lack of effector function and shifting to a Th2 response may not account for the lack of progression to cGN and ESRD in R27 female mice.

Further attempts to discern immune parameter differences between young NZM2328 and R27 mice were not successful

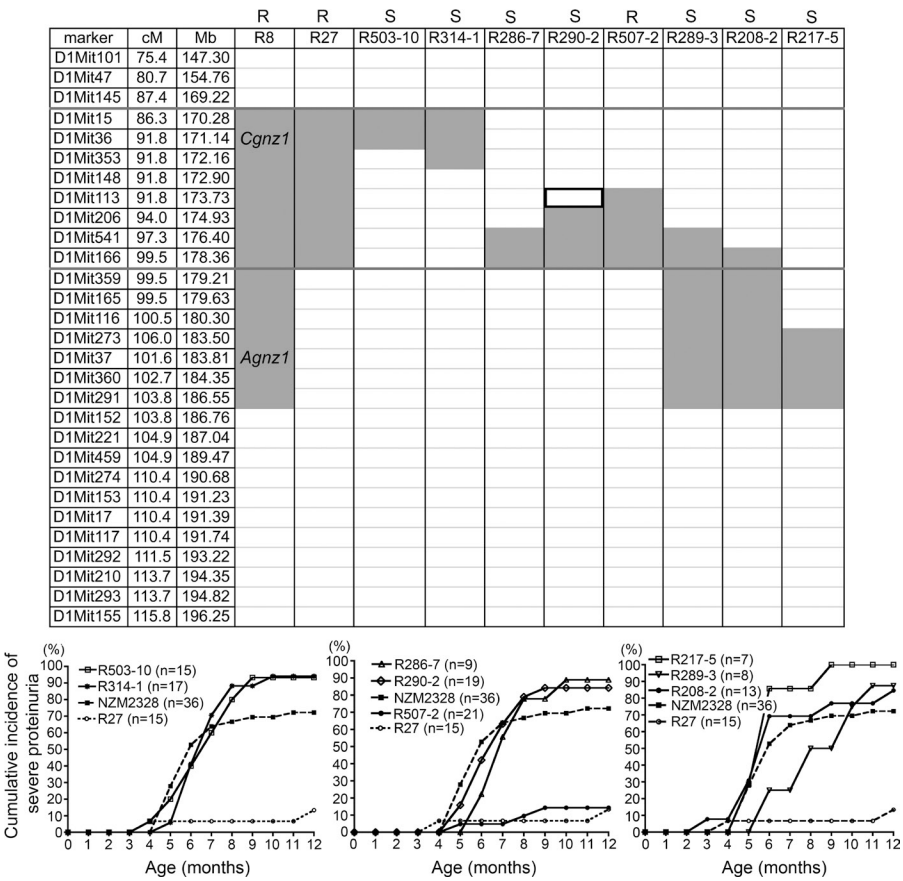

Figure 8. Genetic composition of the distal chromosome 1 of the *Cgnz1* interval–specific and *Agnz1*-specific recombinant congenic strains. Top: the gray bars represent the chromosome 1 segments of C57L/J on NZM2328 background. The listed microsatellite markers were used to determine the boundaries of C57L/J boundaries of the C57L/J fragments. The physical location of the satellite markers are based on mouse assembly NCBIM37. "R" denotes resistance to progression to cGN and "S" means sensitive to this progression. Bottom: cohorts of mice of each intrachromosomal recombinant strains from R27 were monitored for the development of severe proteinuria that is a marker for progression to cGN from aGN. The data on NZM2328 and R27 were included as references. Mice of all recombinant strains except R507-2 progress to cGN as indicated by the similar or greater incidence of severe proteinuria as compared with NZM2328.

in that they have similar numbers of splenic and lymph node activated and nonactivated T and B cells. There was no difference in the B cell signaling pathway as measured by calcium flux induced by B cell receptor activation. No attempts were made to measure these parameters in aged R27 and NZM2328 in view of changes that may be due to disease and not intrinsic to the immune system. The role of T cells in lupus nephritis has been well recognized (Wofsy and Seaman, 1985; Lawson et al., 2001; Tipping and Holdsworth, 2003). Our previous study (Bagavant et al., 2006) has shown that activation and expansion of nephritogenic T cells in regional lymph nodes are associated with progression to renal failure. It was also shown that oligoclonal expansion of T cells was seen both in kidneys and draining lymph nodes. Attempts to determine whether there was similar clonal T cell expansion in R27 were not successful.

Recently, renewed interest has been generated on the role of infiltrating macrophages and dendritic cells in renal diseases (Holdsworth and Tipping, 2007). Relevant to this discussion are the findings by Schiffer et al. (2008) that activated renal macrophages are markers of disease onset and disease remission in lupus nephritis. In addition, a set of inflammatory markers has been identified to be associated with the onset of nephritis. Some of these markers are from activated macrophages and activated endothelial cells. Although there was a trend to have more mRNA encoding these inflammatory markers in the diseased NZM2328 kidneys in comparison with those in R27 kidneys, the differences did not reach statistical significance. In addition, the macrophage and dendritic cell populations in the NZM2328 diseased kidneys were not different from those in the R27 kidneys. More importantly, the unique hybrid mononuclear phagocytes that were marked by F4/80^{high}, CD11c^{int} and expressed proinflammatory, regulatory, and tissue repaired/degradation genes at the onset of nephritis (Bethunaickan et al., 2011) were also present in R27 kidneys. Thus, our data suggest that despite significant inflammation as a result of IC deposition and complement activation, R27 female kidneys are resistant to progression to severe proteinuria and ESRD.

It should be emphasized that R27 mice make anti-kidney Abs at an early age. They also make comparable Ab responses to heterologous sheep IgG. These observations suggest that R27 and NZM2328 mice have a comparable capacity to mount Ab responses to endogenous and foreign antigens. Despite the resistance to end organ damage, R27 mice do have mild proteinuria. It is likely that the resistance to end organ damage allows the clearing of the deposited IC. The accumulation of Ig in the vacuoles in the endothelial cells suggests that endocytosis of the dissolved IC may be a mechanism for clearing of the deposited IC. However, this mechanism has limited capacity in that over a period of time, the cleared IC accumulates in the endothelial cytoplasm as large vesicles. Nevertheless,

Table 2. Representative SLE patients with marked elevated autoantibodies without end organ damage (A), with renal disease and resistance to progression to cGN (B and C), and rapidly progressive renal disease leading to end stage renal failure (D)

Patient	Age	Ethnicity	Initial clinical presentation	Renal disease	Clinical laboratory	Clinical course
A	30	AAF	Age 16 yr gave birth to infant with neonatal lupus with skin involvement.	None.	+ANA, +anti-Ro, La, Sm and RNP Abs, Normal C2, C4 and CH50. Serum IgG 3700 mg/dl, IgA 560 mg/dl, ESR 110 mm/h, normal CRP, normal creatinine.	Asymptomatic.
B	29	Korean	At age 18 yr, she developed skin rash, arthritis with positive serology. She was treated with steroids and was non-compliant.	18 mo after initial presentation, she had trace proteinuria, hematuria. She had skin involvement. At 27 mo, she was found to have marked hematuria, casts, and proteinuria (900 mg per/24 h) with low CI. Renal bx showed class III/V proliferative lupus nephritis.	+ANA, +anti-Ro, La and dsDNA Abs. Marked decrease in C2, C4, and CH50, leukopenia, normal creatinine.	Initial treatment Hydro 400 mg/d, Pred 60 mg/d, and Myco 1,750 mg/d. After 3 mo, no proteinuria and normal C2, C4, and CH50. She became asymptomatic with normal CBC. After 9 mo, Pred was stopped and hematuria was not detected. She has been maintained on Hydro 400 mg/day and Myco 500 mg/d for last six yr without lupus flare.
C	47	Cauc.	At age 42 yr, she had malar rash, arthralgia, fatigue, and fever with positive ANA and anti-dsDNA. She was treated with Hydro and was in remission.	4 yr after initial presentation and 3 mo after discontinuing hydroxychloroquine, she presented with marked arthralgia, malar rash, oral ulcers, and diffuse body pain. She was found to have 3+ proteinuria, marked hematuria, and casts in her urine. She had anemia and thrombocytopenia.	+ANA, +anti-Ro, dsDNA Abs + RF, thrombocytopenia, anemia. Normal renal function.	She was treated with Hydro 400 mg/d, Pred 40 mg/d, and Myco 2 g/d. After 2 mo of treatment, her proteinuria ceased. 1 mo later, hematuria was not detected. Her complements returned to normal. Her anemia and thrombocytopenia were cured. She was tapered off Pred and maintained on Hydro 400 mg/d and Myco 500 mg/d without a flare for the past 4 yr.
D	56	AAF	At age 55 yr, she presented with decreased complements, +ANA, +anti-SmD, +anti-dsDNA, decreased renal function, and CNS disease. Initial renal bx showed class IV proliferative lupus nephritis with moderate CI. She was treated with pulse steroids and monthly high dose Cyclo.	6 mo after presentation and 2 mo of therapy, she was found to have impaired renal function with creatinine 2.4 and severe proteinuria. Repeated renal bx showed marked sclerotic glomeruli with high CI.	+ANA, +anti-Sm, dsDNA Abs, marked decrease C2, C4, and CH50. Creatinine 2.4 mg/dl.	She was not treated and managed symptomatically. 2 yr later, she was begun on dialysis and 3 yr later, she received a renal transplant.

Hydro = hydroxychloroquine, Pred = prednisone, Myco = mycophenolate mofetil, Cyclo = cyclophosphamide, CI = chronicity index, and Cauc. = caucasian.

the resistance of R27 podocytes to damage by IC and complement activation permits the clearance of the IC by this mechanism. As stated above, seven of the nine candidate genes are either mitochondrial genes or genes affecting autophagy and cell survival. One or more of these genes afford podocyte survival so that IC with complement can be cleared.

Genetic evidence supports the hypothesis that autoimmunity and end organ damage are under separate genetic control and have different underlying mechanisms. Attempts to demonstrate this by cell transfer experiments by two different methods were not successful due to technical reasons as stated in the Results section. Our experiment showing that R27 female mice were resistant to the development of experimental GN with a sheep anti–mouse GBM serum supports the stated hypothesis. In addition, in preliminary experiments (unpublished data), young R27 female mice were shown to make ANA and anti-dsDNA antibodies without developing cGN when they were given IFN-α by an adenoviral delivery system. In contrast young NZM2328 female mice treated similarly developed severe proteinuria and early death. Thus enhancing

autoimmunity in R27 does not lead to severe proteinuria and ESRD. Taking all these results into consideration, it is concluded that end organ resistance to cGN development in R27 is an intrinsic property of their kidneys. Although the gene that contributes to the end organ resistance to damage remains to be identified, our current observation gives credence to the thesis that it is important to consider the role of the target organ in elucidating the pathogenesis of autoimmune disorders.

Clinical implications

The basic observations in this investigation have significant clinical implications. To discern these implications, four clinical cases were presented in Table 2. The patient in the first case does not satisfy the diagnostic classification for SLE as set forth by the American college of Rheumatology (Tan et al., 1982; Hochberg, 1997), indicating that serological abnormalities that result from autoimmune responses cannot and should not be confused with end organ damage. In a recent publication, Satoh et al. (2012) obtained data that show ∼13.8 (12.2–15.5)% of normal adults have positive ANA and this ratio is relatively constant for populations with each decade of increasing ages to 70 yr. This finding suggests that ANA is common irrespective of age. The lack of increases in the prevalence of ANA with age suggests that ANA is likely to be transiently positive in the population. This finding supports the conclusion that breaking tolerance to nuclear antigens should not be construed as an indicator for the development of autoimmune disease.

Recently, a dominant recessive form of SLE has been reported in six Arab families (Al-Mayouf et al., 2011). A loss-of-function variant in *DNASE1L3* was found in these families. Of 27 offspring, 17 were diagnosed to have SLE. 11 of them have nephritis with hypocomplementemia. One of these patients with nephritis had no detectable anti-dsDNA antibodies. The other six individuals had positive ANA and anti-dsDNA antibodies and hypocomplementemia without nephritis. Despite consanguinity and the presence of lupus nephritis in at least one sibling and marked serological abnormalities, the phenotype of the six individuals with the diagnosis of SLE and without nephritis suggests the presence of genes that are capable of conferring resistance to kidney damage. Relevant to this discussion is a group of patients with SLE and kidney abnormality without overt clinical data to suggest renal involvement. These patients are classified as SLE patients with silent nephritis (Dooley, 2011). In the largest series of these patients, Mahajan et al. (1977) reported the follow-up of 27 SLE patients who were biopsied without significant clinical renal abnormalities. The mean follow-up was 3.6 yr. 12 of the 27 patients were found to have diffuse proliferative GN. 1 of these 12 patients died of renal failure 5 yr after the diagnosis, and 1 died of sepsis, while the remaining 10 remained stable without evidence of renal diseases, indicating that the progression of lupus GN is not inescapable and that this progression may be very slow in a substantial number of patients.

The observation that genes that confer end organ resistance may be important in our understanding of pathogenesis of lupus GN provides a logical explanation for the highly variable clinical presentations in SLE. This is an impetus to rekindle the discussion whether all patients should be treated and cared for by a consensus treatment guideline as proposed recently (Hahn et al., 2012). It is clear that those individuals with genes conferring resistance to end organ damage, presumably as in the cases B and C, should not have same treatments as those without these genes as in case D; more vigorous treatments may be required in the latter case. As more understanding of the genetic and environmental factors that influence the clinical course of SLE in general and lupus GN in particular is achieved, individualized treatments should be considered to minimize side effects and to maximize therapeutic results. In this regard, the present investigation has significant clinical implications.

The concept of end organ resistance to damage has general applications in medicine in addition to lupus GN. The variable clinical presentations and responses to therapy in other autoimmune diseases, such as rheumatoid arthritis, psoriatic arthritis, ankylosing spondylitis, and multiple sclerosis can be explained by this concept. Other non-autoimmune disorders, such as osteoarthritis and diabetic neuropathy, that have variable clinical courses could also be due to the variation of the target organs to resist damage. Thus, in clinical medicine this concept should be stressed in dealing with individual patients.

Human homologue to mouse Cgnz1

Cgnz1 is located on the distal mouse chromosome 1qH3. In addition to *Cgnz1*, the distal region of chromosome 1 has been reported in other studies to be associated with lupus nephritis (Morel, 2012). The distal region of mouse chromosome 1 is an important region for lupus GN susceptibility. A nearly identical homologous region exists on human chromosome 1g23 from 160.0 to 161.6 Mb. With the exception of *LOC10041098*, each of the mouse genes in *Cgnz1* region has a human counterpart as the homologous region. The exact gene order is preserved between the two species. Thus, the human homologue of *Cgnz1* has not been implicated in human genetic studies on lupus susceptibility. This may be due to the bias toward autoimmunity in previous studies. The conserved gene order suggests similar function in man and provides a rationale for more detailed interrogation of this region in human lupus. Studies of this region in man may identify candidate genes for *Cgnz1* and may provide biomarkers that may be important for designing an individualized therapeutic approach.

MATERIALS AND METHODS

Animals. NZM2328 and C57L/J breeding pairs were originally obtained from The Jackson Laboratory. All mice were housed under a pathogen-free environment at the University of Virginia Animal Care Facility. NZM2328.C57L/Jc1 (Lc1) congenic line was generated using a microsatellite marker-assisted speed congenic generation protocol as described in Waters et al. (2004). Mice were kept at the University of Virginia Center of Comparative Medicine under pathogen-free conditions. Animal experimental protocols

were approved by the Institutional Animal Care and Use committee. Animals were used in a manner in full accordance with federal regulations (PHS Policy and Animal Welfare Act).

Intrachromosomal 1 recombinant strains. (Lc1XNZM2328)F1XNZM2328 progeny were screened using a dense panel of chr.1 polymorphic microsatellite markers (Fig. 1). Mice with recombination within the Lc1 region were selected. Heterozygous founder mice were crossed with NZM2328, and the F1 mice were intercrossed to generate the homozygous recombinant lines. In this study, all mice used were homozygous females.

Phenotypic characterization. Cohorts of homozygous female mice of R8 and R27 were followed to 12 mo of age. Additional cohorts of R27 mice were followed to 15 mo of age. Their urinary protein concentrations were examined twice a month semiquantitatively using dipsticks (Bayer Multistix 10 SG). Severe proteinuria was diagnosed when mice had a readout of +++ or above (>300 mg/dl). Mice were dissected either at the time of developing severe proteinuria or at 12–15 mo of age. R27 female mice of different ages were also dissected for various studies such as serological assays and histological studies.

Serological assays. IgG anti-dsDNA antibody concentrations in terminal sera of R27 and the recombinant strains were measured by ELISA as previously described (Waters et al., 2001). In brief, photobiotinylated pGEM-3z dsDNA was used as substrate and was bound to Immulon 4HB plates (Dynex Technologies) precoated with streptavidin. Serum samples were titered with serial dilution starting at 1:50 in 3% BSA in PBS with 0.05% Tween 20 and then incubated on plates for 2 h at room temperature. After washing, goat anti–mouse IgG-HRP was added and incubated for 2 h, followed by *o*-phenylene diamine in citrate phosphate buffer for 30 min. OD at 490 nm was measured. Sera were regarded as positive if their anti-dsDNA antibody concentrations were higher than the mean concentration of 12-mo-old C57L/J female mice plus 2 SD. IgG ANA were examined by indirect immunofluorescence microscopy using NIH/3T3 cells as substrates (Waters et al., 2004). Sera were diluted 1:50 and goat anti–mouse rhodamine-conjugated IgG was used as the secondary antibody.

Kidney histology. Kidneys of female mice of NZM2328, R27, and the recombinant strains were collected and fixed in 10% neutral-buffered formalin at the time of dissection. After embedding, formalin-fixed kidneys were sectioned at 2 μm and stained with hematoxylin/eosin (H&E), periodic acid-Schiff (PAS), and/or oil red O. aGN and cGN were scored in a blinded fashion using a scale of 0 to 5. aGN scores were given based on the severity of glomerular hypercellularity, mesangial matrix expansion, focal necrosis, and epithelial cell crescents. cGN scores were given based on the severity of glomerulosclerosis (focal to global), tubular atrophy, dilated tubules with hyaline casts, and interstitial fibrosis (Waters et al., 2001).

Immunofluorescence staining. For evaluation of glomerular Ig and C3 deposition, frozen sections of mouse kidneys were fixed in methanol at −20°C for 10 min, blocked with 2% normal goat serum in PBS containing 3% BSA, and then stained with FITC conjugated goat anti–mouse IgM, goat anti–mouse IgA, goat F(ab') 2 anti–mouse IgG, goat anti–mouse IgG1, goat anti–mouse IgG2a, goat anti–mouse IgG2b, and goat anti–mouse C3 antibodies. Deposits in the glomeruli were evaluated using a semi-qualitative scale of 0–4, where 0 denotes no deposits, and the analysis was done by a scorer blinded to the identification of the mice. For confocal immunofluorescence staining, methanol-fixed 4-μm frozen kidney sections were blocked with 2.4G2 monoclonal antibody to FcγIII/II receptors in PBS containing normal goat serum and 3% BSA. Purified rabbit anti–mouse collagen IV was used as primary antibody and incubated for 2 h. After washing, goat anti–mouse IgG FITC and goat anti–rabbit Alexa Fluor 546 antibodies were incubated for 1 h.

TEM. Kidneys in mice were perfused with PBS and fixed by immersion at 4°C overnight in a solution containing 4% (wt/vol) paraformaldehyde and 2.5% (wt/vol) glutaraldehyde in 0.1 M phosphate buffer, pH 7.4. The samples were equilibrated to room temperature, washed in distilled water, and post-fixed for 1 h in 1% (wt/vol) osmium tetroxide + 0.01% potassium ferrocyanide. After washing in distilled water, the samples were dehydrated in 70 and 100% acetone, infiltrated with and embedded in epoxy resin (EPON; Electron Microscopy Sciences, Inc.), and polymerized at 60°C for 48 h. Ultrathin sections (70–80 nm in thickness), prepared on an ultramicrotome (Ultracut UCT; Leica) using a Diatome diamond knife, were collected on 200 mesh copper grids and contrast stained with lead citrate and uranyl acetate according to routine procedures. The sections were examined in a transmission electron microscope (1230; JEOL) operating at 80 KV and equipped with a digital camera (12-C; Scientific Instruments and Applications, Inc.).

Measurement of serum immunoglobulin concentrations. Concentrations of serum IgM, IgG, IgG1, IgG2a, and IgG2b of R27 and NZM2328 mice were determined by ELISA. Immulon 4HB plates were coated with purified goat anti–mouse IgM, IgG, IgG1, IgG2a, and IgG2b at 4°C overnight. After washing with PBS with 0.05% Tween 20 and then blocking with 5% BSA in PBS with 0.05% Tween 20 for 1 h, serum samples that were diluted 1:40 and 1:160 in 1% BSA in PBS with 0.05% Tween 20 were incubated on plates for 2 h at room temperature. After washing, HRP-conjugated goat anti–mouse IgM, IgG, IgG1, IgG2a, or IgG2b was added and incubated for 2 h. After washing, *o*-phenylene diamine in citrate phosphate buffer was incubated for 30 min. OD at 490 nm was measured and the serum immunoglobulin concentrations were calculated based on standard curves.

Measurement of blood urea nitrogen and creatinine. Blood urea nitrogen levels in NZM2328 and R27 sera were measured as follows. In brief, sera were deproteinized using 3% trichloroacetic acid. Supernatants were mixed with BUN color reagent and acid reagent, and then boiled for 10 min. OD at 535 nm was read and BUN levels were calculated based on standard curves. Serum creatinine was measured by a modified Jaffe method (Keppler et al., 2007).

Measurement of urinary albumin. Spot urine samples were collected from NZM2328 and R27 female mice and were spun down before testing. Urinary albumin levels were determined by indirect competitive ELISA using Albuwell M kit according to manufacturer's protocol. In brief, urine supernatants were diluted at 1:13 and incubated for 30 min with rabbit anti–mouse albumin antibodies. After washing, anti–rabbit HRP was added and incubated for 30 min. After color development, OD at 450 nm was measured and albumin levels were calculated based on standard curves.

Isolation of B cells and measurements of anti-IgM induced influx of intracellular Ca^{2+}. B cells were isolated from spleens of 2–3-mo-old NZM2328 and R27 female mice using negative selection with anti-biotin microbeads (Miltenyi Biotec) according to manufacturer's protocol. Anti–mouse IgM antibody induced calcium flux was measured on isolated B cells by the Indo-2 method as described previously (Bjorndahl et al., 1989).

Total RNA isolation and real-time PCR. Total RNA was isolated from splenic B cells and $CD4^+$ T cells using RNeasy Mini kit (QIAGEN). cDNA was synthesized using SuperScript III First-Strand Synthesis System for RT-PCR (Life Technologies). Amplification was performed in duplicate using ABsolute QPCR SYBR Green Fluorescein (Thermo Fisher Scientific), and the primers for cytokines, chemokines, and their receptors were from Schiffer et al. (2008) in an iQ5 Multicolor Real-Time PCR Detection system (Bio-Rad Laboratories). Annealing temperature was 60°C for all the primers. Melting curve analysis confirmed that there was only one specific amplification product for each primer pair.

Preparation of single cell suspensions and flow cytometry. Kidney single cell suspensions were prepared from mice perfused through the right ventricle with saline. Dissected kidneys were minced and incubated in 133 U/ml Blendzyme 2 (Roche) for 15–30 min and further dispersed by pipetting.

Residual red blood cells were lysed by hypotonic saline and debris was filtered through 40-µm nylon sieves. Splenocytes and mononuclear cells from lymph nodes were similarly prepared. Cells were pretreated with blocking anti-FcγRII/FcγRIII mAb 2.4G2, stained with fluorophore-conjugated mAb, and analyzed by flow cytometry using FACSCalibur (BD) with multicolor upgrade to a three-laser (488-, 637-, and 407-nm lines) and eight-detection-channel system (Cytek). Dead cells were excluded from analysis by DAPI (Roche) staining.

All mAbs used in flow cytometry were from BioLegend, except eFlour-conjugated mAb which were from eBioscience. Antibodies to CD4, CD8, and CD3 were used to characterize T cells. Anti-CD19 Ab was used to detect B cells. Anti-CD69 and anti-CD86 Abs were used to detect activated T and B cells, respectively. For macrophage and dendritic cell analyses, tissue digests were stained with anti–Ly6c-FITC, anti–CD103-PE, anti–I-A-PerCP-eFluor710, anti–CD11b-PE-Cy7, anti–F4/80–Alexa Fluor 647, anti–CD11c–APC–eFluor 780, and DAPI. For other cell types, single cell suspensions were stained with anti–CD8-FITC, anti–B220-PE, anti–CD3-PerCP-eFluor710, anti–Thy1.2-PE, anti–NK1.1–Alexa Fluor 647, anti–CD4-APC-eFluor780, and DAPI. Neutrophils are distinguishable as a $Ly6c^{high}CD11b^{high}$ population. Samples were acquired on a FACScan (BD), and data were collected with CellQuest (BD) and analyzed with FlowJo (Tree Star) software.

Induction of sheep anti-GBM nephrotoxic nephritis. Mouse glomeruli were isolated by sequential sieving. Glomeruli were frozen and then sonicated to obtain the glomerular extract that was used for the preparation of sheep nephrotoxic serum (NTS; Lampire Biological Products Ltd). Sheep NTS was characterized for reactivity to mouse GBM. Mice were housed in metabolic cages for 24 h and urine was collected. This was followed by i.p. injection with NTS (75 µl/mouse). Urine was collected on days 7, 14, 21, and 28 after injection and the experiment terminated. Kidneys and sera were collected at the time of sacrifice. Urinary albumin and creatinine were measured as stated above. Deposition of NTS was confirmed by staining of frozen kidney sections with biotinylated rabbit anti–sheep IgG (SouthernBiotech), followed by Streptavidin Alexa Fluor 647. Glomerular deposits of mouse IgG were studied on frozen sections of kidney using sheep anti-mouse IgG FITC conjugate (SouthernBiotech). This procedure assays both acute and cGN in the treated mice.

Statistical analysis. Two-tailed unpaired Student *t* tests and two-tailed Fisher's unpaired tests were performed to evaluate significance of the results with assigned p-values.

Online supplemental material. Table S1 summarizes serum IgM, IgG, and IgG subclass concentrations of NZM2328 and R27 at different ages. Table S2 deals with lymphocyte subpopulations of spleen and kidney draining lymph nodes. Table S3 gives the genes that are located within the *Cgnz1* refined genetic region. Table S4 provides information on nine candidate genes for *Cgnz1*. Online supplemental material is available at http://www.jem.org/cgi/content/full/jem.20130731/DC1.

The authors thank Dr. Michael G Brown in the Department of Medicine at the University of Virginia for his advice for breeding experiments during the early stage of this study. They thank Dr. John Kung of the Institute of Molecular Biology, Academia Sinica Taipei, Taiwan for his help in sequencing the BAC clones of NZM2328 covering the 1.34 Mb region where *Cgnz1* is located. The authors thank Lena Garrison for her help in preparing the manuscript.

This work was supported by grants P50-AR04522, R01-AR047988, and R01-AR049449 from the National Institute of Arthritis and Musculoskeletal and Skin Diseases, and R01-AI079621 from the National Institute of Allergy and Infectious Diseases and grants from Alliance for Lupus Research.

The authors have no conflicting financial interests.

Submitted: 8 April 2013
Accepted: 6 September 2013

REFERENCES

Al-Mayouf, S.M., A. Sunker, R. Abdwani, S.A. Abrawi, F. Almurshedi, N. Alhashmi, A. Al Sonbul, W. Sewairi, A. Qari, E. Abdallah, et al. 2011. Loss-of-function variant in DNASE1L3 causes a familial form of systemic lupus erythematosus. *Nat. Genet.* 43:1186–1188. http://dx.doi.org/10.1038/ng.975

Bagavant, H., U.S. Deshmukh, H. Wang, T. Ly, and S.M. Fu. 2006. Role for nephritogenic T cells in lupus glomerulonephritis: progression to renal failure is accompanied by T cell activation and expansion in regional lymph nodes. *J. Immunol.* 177:8258–8265.

Bethunaickan, R., C.C. Berthier, M. Ramanujam, R. Sahu, W. Zhang, Y. Sun, E.P. Bottinger, L. Ivashkiv, M. Kretzler, and A. Davidson. 2011. A unique hybrid renal mononuclear phagocyte activation phenotype in murine systemic lupus erythematosus nephritis. *J. Immunol.* 186:4994–5003. http://dx.doi.org/10.4049/jimmunol.1003010

Bjorndahl, J.M., S.-S.J. Sung, J.A. Hansen, and S.M. Fu. 1989. Human T cell activation: differential response to anti-CD28 as compared to anti-CD3 monoclonal antibodies. *Eur. J. Immunol.* 19:881–887. http://dx.doi.org/10.1002/eji.1830190515

Clynes, R., C. Dumitru, and J.V. Ravetch. 1998. Uncoupling of immune complex formation and kidney damage in autoimmune glomerulonephritis. *Science.* 279:1052–1054. http://dx.doi.org/10.1126/science.279.5353.1052

Dooley, M.A. 2011. Clinical manifestations of lupus nephritis. *In* Lupus Nephritis, second edition. E.J. Lewis, M.M. Schwartz, S.M. Korbet, and D.T.M. Chan, editors. Oxford University Press, New York. 1–34.

Hahn, B.H., M.A. McMahon, A. Wilkinson, W.D. Wallace, D.I. Daikh, J.D. Fitzgerald, G.A. Karpouzas, J.T. Merrill, D.J. Wallace, J. Yazdany, et al; American College of Rheumatology. 2012. American College of Rheumatology guidelines for screening, treatment, and management of lupus nephritis. *Arthritis Care Res.* (*Hoboken*). 64:797–808. http://dx.doi.org/10.1002/acr.21664

Hochberg, M.C. 1997. Updating the American College of Rheumatology revised criteria for the classification of systemic lupus erythematosus. *Arthritis Rheum.* 40:1725. http://dx.doi.org/10.1002/art.1780400928

Holdsworth, S.R., and P.G. Tipping. 2007. Leukocytes in glomerular injury. *Semin. Immunopathol.* 29:355–374. http://dx.doi.org/10.1007/s00281-007-0097-9

Jacob, C.O., L. Pricop, C. Putterman, M.N. Koss, Y. Liu, M. Kollaros, S.A. Bixler, C.M. Ambrose, M.L. Scott, and W. Stohl. 2006. Paucity of clinical disease despite serological autoimmunity and kidney pathology in lupus-prone New Zealand mixed 2328 mice deficient in BAFF. *J. Immunol.* 177:2671–2680.

Keppler, A., N. Gretz, R. Schmidt, H.-M. Kloetzer, H.-J. Groene, B. Lelongt, M. Meyer, M. Sadick, and J. Pill. 2007. Plasma creatinine determination in mice and rats: an enzymatic method compares favorably with a high-performance liquid chromatography assay. *Kidney Int.* 71:74–78. http://dx.doi.org/10.1038/sj.ki.5001988

Kumar, K.R., L. Li, M. Yan, M. Bhaskarabhatla, A.B. Mobley, C. Nguyen, J.M. Mooney, J.D. Schatzle, E.K. Wakeland, and C. Mohan. 2006. Regulation of B cell tolerance by the lupus susceptibility gene Ly108. *Science.* 312:1665–1669. http://dx.doi.org/10.1126/science.1125893

Lawson, B.R., S.I. Koundouris, M. Barnhouse, W. Dummer, R. Baccala, D.H. Kono, and A.N. Theofilopoulos. 2001. The role of alpha beta+ T cells and homeostatic T cell proliferation in Y-chromosome-associated murine lupus. *J. Immunol.* 167:2354–2360.

Mahajan, S.K., N.G. Ordóñez, P.J. Feitelson, V.S. Lim, B.H. Spargo, and A.I. Katz. 1977. Lupus nephropathy without clinical renal involvement. *Medicine* (*Baltimore*). 56:493–501.

Mohan, C., E. Alas, L. Morel, P. Yang, and E.K. Wakeland. 1998. Genetic dissection of SLE pathogenesis. Sle1 on murine chromosome 1 leads to a selective loss of tolerance to H2A/H2B/DNA subnucleosomes. *J. Clin. Invest.* 101:1362–1372.

Morel, L. 2012. Mapping lupus susceptibility genes in the NZM2410 mouse model. *Adv. Immunol.* 115:113–139. http://dx.doi.org/10.1016/B978-0-12-394299-9.00004-7

Morel, L., U.H. Rudofsky, J.A. Longmate, J. Schiffenbauer, and E.K. Wakeland. 1994. Polygenic control of susceptibility to murine systemic

lupus erythematosus. *Immunity*. 1:219–229. http://dx.doi.org/10.1016/1074-7613(94)90100-7

Morel, L., B.P. Croker, K.R. Blenman, C. Mohan, G. Huang, G. Gilkeson, and E.K. Wakeland. 2000. Genetic reconstitution of systemic lupus erythematosus immunopathology with polycongenic murine strains. *Proc. Natl. Acad. Sci. USA*. 97:6670–6675. http://dx.doi.org/10.1073/pnas.97.12.6670

Morel, L., K.R. Blenman, B.P. Croker, and E.K. Wakeland. 2001. The major murine systemic lupus erythematosus susceptibility locus, Sle1, is a cluster of functionally related genes. *Proc. Natl. Acad. Sci. USA*. 98:1787–1792. http://dx.doi.org/10.1073/pnas.98.4.1787

Rahman, A., and D.A. Isenberg. 2008. Systemic lupus erythematosus. *N. Engl. J. Med*. 358:929–939. http://dx.doi.org/10.1056/NEJMra071297

Satoh, M., E.K. Chan, L.A. Ho, K.M. Rose, C.G. Parks, R.D. Cohn, T.A. Jusko, N.J. Walker, D.R. Germolec, I.Z. Whitt, et al. 2012. Prevalence and sociodemographic correlates of antinuclear antibodies in the United States. *Arthritis Rheum*. 64:2319–2327. http://dx.doi.org/10.1002/art.34380

Schiffer, L., R. Bethunaickan, M. Ramanujam, W. Huang, M. Schiffer, H. Tao, M.P. Madaio, E.P. Bottinger, and A. Davidson. 2008. Activated renal macrophages are markers of disease onset and disease remission in lupus nephritis. *J. Immunol*. 180:1938–1947.

Shimizu, S., N. Sugiyama, K. Masutani, A. Sadanaga, Y. Miyazaki, Y. Inoue, M. Akahoshi, R. Katafuchi, H. Hirakata, M. Harada, et al. 2005. Membranous glomerulonephritis development with Th2-type immune deviations in MRL/lpr mice deficient for IL-27 receptor (WSX-1). *J. Immunol*. 175:7185–7192.

Tan, E.M., A.S. Cohen, J.F. Fries, A.T. Masi, D.J. McShane, N.F. Rothfield, J.G. Schaller, N. Talal, and R.J. Winchester. 1982. The 1982 revised criteria for the classification of systemic lupus erythematosus. *Arthritis Rheum*. 25:1271–1277. http://dx.doi.org/10.1002/art.1780251101

Theofilopoulos, A.N., and F.J. Dixon. 1985. Murine models of systemic lupus erythematosus. *Adv. Immunol*. 37:269–390. http://dx.doi.org/10.1016/S0065-2776(08)60342-9

Tipping, P.G., and S.R. Holdsworth. 2003. T cells in glomerulonephritis. *Springer Semin. Immunopathol*. 24:377–393. http://dx.doi.org/10.1007/s00281-003-0121-7

Tsokos, G.C. 2011. Systemic lupus erythematosus. *N. Engl. J. Med*. 365:2110–2121. http://dx.doi.org/10.1056/NEJMra1100359

Ward, M.M. 2009. Changes in the incidence of endstage renal disease due to lupus nephritis in the United States, 1996-2004. *J. Rheumatol*. 36:63–67.

Waters, S.T., S.M. Fu, F. Gaskin, U.S. Deshmukh, S.-S.J. Sung, C.C. Kannapell, K.S.K. Tung, S.B. McEwen, and M. McDuffie. 2001. NZM2328: a new mouse model of systemic lupus erythematosus with unique genetic susceptibility loci. *Clin. Immunol*. 100:372–383. http://dx.doi.org/10.1006/clim.2001.5079

Waters, S.T., M. McDuffie, H. Bagavant, U.S. Deshmukh, F. Gaskin, C. Jiang, K.S. Tung, and S.M. Fu. 2004. Breaking tolerance to double stranded DNA, nucleosome, and other nuclear antigens is not required for the pathogenesis of lupus glomerulonephritis. *J. Exp. Med*. 199:255–264. http://dx.doi.org/10.1084/jem.20031519

Wofsy, D., and W.E. Seaman. 1985. Successful treatment of autoimmunity in NZB/NZW F1 mice with monoclonal antibody to L3T4. *J. Exp. Med*. 161:378–391. http://dx.doi.org/10.1084/jem.161.2.378

Xie, C., X.J. Zhou, X. Liu, and C. Mohan. 2003. Enhanced susceptibility to end-organ disease in the lupus-facilitating NZW mouse strain. *Arthritis Rheum*. 48:1080–1092. http://dx.doi.org/10.1002/art.10887

Xie, C., Y. Du, K. Kumar, L. Li, J. Han, K. Liu, X.J. Zhou, and C. Mohan. 2013. Lupus-prone strains vary in susceptibility to antibody-mediated end organ disease. *Genes Immun*. 14:170–178. http://dx.doi.org/10.1038/gene.2012.57